A Deformable Membrane for the Segmentation of Cytological Samples

Volker Metzler, Jörg Bredno, Thomas Lehmann, Klaus Spitzer

Institute of Medical Informatics
Aachen University of Technology (RWTH)
D–52074 Aachen, Germany

ABSTRACT

In clinical cytology quantitative parameters have to be extracted from a large number of biological samples to obtain diagnostically relevant and reproducible information. Computer–assisted microscopy can provide methods that increase the quality and comparability of clinical studies by reducing the subjective influence of human operators on their results. In order to guarantee the correctness of extracted parameters automatic and reliable segmentation of the samples is required. For the detection of cytological objects a novel deformable membrane model is presented which is strictly based on macroscopical mechanics and statics. This is appropriate for modeling physiological membranes, because their shape is determined exclusively by mechanical forces. The self–driven membrane converges iteratively towards a stable state, where the contrary forces are in balance. However, active contours may not yield sufficient detection quality for acquisition of quantitative parameters. Therefore, after convergence a stochastic optimization process corrects the contour according to local graylevel information. This yields a contour that is well–adapted to the local graylevel structure. Additionally, for subsequent cytometric quantifications a local measure of confidence is provided for the contour. This can be used to enhance the robustness of the extracted parameters by incorporating the confidence factors in the quantification process. The method is applied to cytological and histological samples of different magnification.

Keywords: Image segmentation, object detection, contour detection, active contours, deformabel membrane, quantitative microscopy, cytological samples

1. INTRODUCTION

The extraction and quantification of parameters from given image material is a common application of image processing in medical research, especially in clinical histology and cytology.[1,2] For clinical screening, features like compactness, local curvature, or densities of cells have to be measured quantitatively in large numbers of samples and assigned to diagnostic evaluations, such as aberrations of cell morphology caused by toxic influences.

The advantages of computer–assisted analysis of biological samples, compared to common methods like interactive measuring or visual evaluation followed by verbal description of the inspected pathological effects are obvious[3]:

- The subjective influence of human observers on the results of cytological studies is reduced. This yields objective experimental data that was obtained in a reproducible way. Such studies are statistically far more relevant than their qualitative counterparts.
- The objective data of quantitative studies becomes comparable to other results and among different sites. The effects of certain expermimental parameters can be studied more exactly because the results are subject to verification.
- Researchers are released from erroneous and time consuming routine work. But still, they have to control the automatic analysis to be able to interprete the quantitative results correctly.

Send correspondence to: Volker Metzler, Institut für Medizinische Informatik, RWTH Aachen, D-52057 Aachen, Germany
E–mail:metzler@imib.rwth-aachen.de, Phone:+49-241-80-88382, FAX:+49-241-8888-426

Part of the SPIE Conference on Image Processing • San Diego, California • February 1998
SPIE Vol. 3338 • 0277-786X/98/$10.00

If the histological tissue was acquired with suitable resolution and appropriate staining, two main steps have to be performed by an automated quantification of relevant features[4]:

- ▷ The main task in computer–assisted microscopy is the segmentation of the images to obtain the objects to be quantified. Hence, segmentation yields the region–of–interest for further feature extraction. This step is of major importance, because the robustness and significance of the parameters depends on the quality of the segmentation.[5]
- ▷ The feature extraction, as second processing step, should extract a broad variety of robust parameters, that allow the clear discrimination between different diagnostic classes.

Hence, to guarantee correct results automatic and reliable segmentation of the samples is required. The detection of complete cell bodies in cytological samples is a demanding task, due to the complex domain and the usual, microscopy–specific, difficulties in modelling geometric or photometric a–priori information.[6]

Many sophisticated segmentation methods have been developed in order to analyse microscopic structures in quantitative cytology.[7–9] But in many cases, variants of thresholding techniques are used.[6,10,11] Their major disadvantage is the pixel–based behaviour, which requires post–processing steps to reduce noise, link unconnected contour segments to obtain clear discrimination between object and background. Especially for very irregular object contours, such methods often yield unsatisfying results. Object–oriented approaches, like active contour models seem to be more appropriate, because they yield closed contours of the objects of interest.[12]

An active contour C consists of a set of vertices V_i connected by edges $\vec{d}_i$. The aim is to contract C until it meets the border of an object. This dynamic behaviour is generated by applying contrary forces on the vertices V_i which are superposed and affect a movement of a vertice. The forces are devided into external (gradient–) forces F_g, that result from local gradients of the image, and internal (deformation–) forces F_d, that result from contour specific effects like local surface tension or curvature. F_g and F_d are directed in oposite. The movement of a vertex is proportional to the weighted sum $F_{\text{tot}} = w_d F_d + w_g F_g$ that is applied to it. This iterative process continues until the contrary forces are in balance, that is when the algorithm converges and the contour has reached its final position.

Today, active contours and deformable models are very popular approaches in medical image processing.[12–14] This results from their special properties:

- ▷ The dynamic influence of each single vertex on its neighbours results in an interpolation of an object's contour at segments with weak gradient information. Local ambiguities can be resolved by this behavour.
- ▷ Compared to edge–based segmentation, the additional linkage of edge segments is not required.
- ▷ The approach is computationally efficient, because the global behaviour is achieved by local manipulations. Additionally, the object–oriented approach to define a contour as a list of vertices makes the administration easy and fast.
- ▷ It is an intuitive approach to object detection and therefore easy to understand.

In this paper a deformable membrane model is presented, that is specially adapted to the segmentation of microscopic biological objects (Sec. 2). The model is exclusively based on macroscopic mechanics and statics, which turned out to be suitable for the segmentation of cytological objects, whose natural shape is determined by the same principles. This includes that a model for elasticity is not needed, because a biological membrane is van–der–Waals bonded.

To support subsequent quantifications, a fuzzy–like measure of local detection quality is provided. These confidence factors enable to distinguish between perfect and poor contour parts, which can be utilized to increase the robustness of quantitative parameters (Sec. 3). Examples for subsequent parameter extraction are given in Sec. 4.

2. CONTOUR DETECTION

The detection of cytological structures by the deformable membrane model is subdevided into four modules. After the removement of microscope–dependent misleading artefacts (Sec. 2.1), the image–dependent external energy is modeled individually for each image (Sec. 2.2). Based on this information, the actual contour detection can be performed by the deformable membrane in the corrected image (Sec. 2.3). The last module enhances the determined contour by a stochastic adaptation (Sec 2.4).

2.1. Removement of artefacts

Light microscopes often have minor soilings in their optical path. To obtain optimal detection results, such artefacts are removed prior to segmentation, because they introduce gradients in the image that may lead to detection errors.

To perform the error correction, the algorithm gets the original sample I_{ori} and an empty image I_{emp} that displays the artefacts in the optical path of the used light microscope. The artefacts are determined by a binarisation of the empty image I_{emp} by applying Otsu's well known global thresholding technique,[15] which yields the binary artefact image I_{art}. To compensate minor translations of the optics, the binary image I_{art} is dilated by a circular structuring element of diameter 3, before the artefacts ($I_{\text{art}}(i,j) = 1$) are removed from the sample I_{ori}. If the contour to be detected is darker than the surrounding histological tissue, this is done by replacing them by the maximum of $I_{\text{ori}}(i,j)$ and the mean graylevel $\mu(I_{\text{ori}})$ of the sample. Therefore, pixels that are sufficiently dark ($I_{\text{ori}}(i,j) \leq \mu(I_{\text{ori}})$) are preserved. In such cases the sample is not manipulated, in order to keep the original information. If the contour is lighter than the surrounding histological tissue (to be set by an external parameter), the mimimum of $I_{\text{ori}}(i,j)$ and $\mu(I_{\text{ori}})$ is replacing the original pixel. The described artefact correction is shown in Fig. 1.

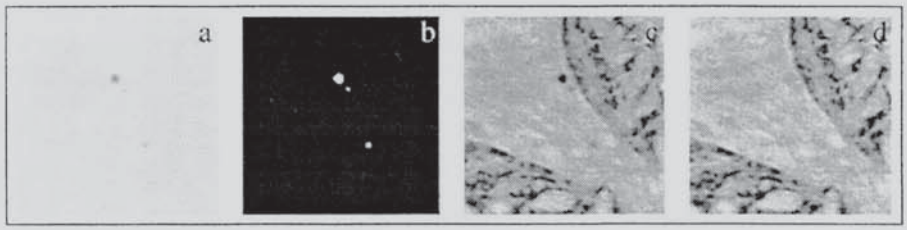

Figure 1. The empty image I_{emp} (a) shows the artefacts that result form soilings in the optical path of the microscope. The binarized artefact image I_{art} (b) yields those pixels that have to be corrected in the cytological sample I_{ori} (c). The corrected image, with removed artefacts I_{cor} is shown in (d).

Of course, the artefact image I_{art} has to be recalculated for each alternation or replacement of the microscope in use. Furthermore, the deformable membrane requires images with sufficiently high contrasts, which is emphasized by a histogram stretching of the input image I_{ori}.

2.2. Generation of Energy Levels

The external energy is modeled individually to the corrected cytological sample I_{cor} by the generation of a table, that assigns an energy level $l(g)$ to each graylevel g.

Usually the external force F_g^i at vertex V_i is proportional to the gradient at V_i. This is a rather unspecific way to impose forces to vertices. This works only if the object's border is the lightest/darkest and the majority of gradients is pointing towards this graylevel maximum/minimum (despite of some noisy gradients and local optima). For cytological samples this is unsuitable, because the object's boundary doesn't necessarily represent the lightest/darkest part of the image (Fig. 2a). In order to keep the algorithm flexible the image has to be analysed before the graylevels $0 \leq g \leq 255$ can be mapped to energy levels $l(g)$, that are transformed to the external force F_g during the contour detection. Starting from a user defined origin (a pixel that lies within the object) a number of radial test profiles $b(r_\varphi)$ are read, which contain the linear interpolated graylevels along the profile with angle φ. On each of these signals $b(r_\varphi)$ the most likely intersection point is determined, where the profile crosses the boundary.

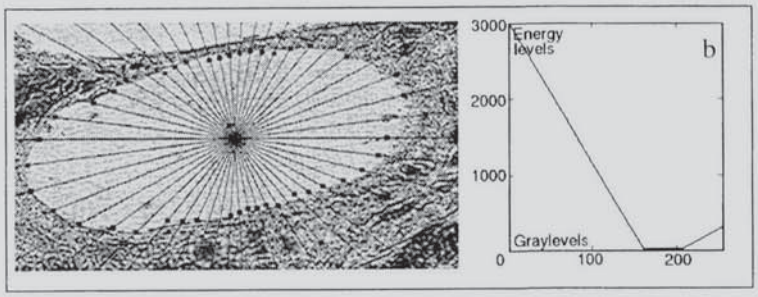

Figure 2. The cytological sample superimposed with the analysed profiles $b(r_\varphi)$ and the proposed intersection points is shown in (a). The diagramm (b) shows the mapping from graylevels to energy levels $l(g)$ that results from this analysis.

In fact, the determination of these intersection propabilities is a simple preliminary contour detection, which yields important information on the object's graylevel structure to be used in the detection phase (Sec. 2.3). For each pixel r on $b(r_\varphi)$ three criteria are analysed. The mean graylevel $\mu(r)$ and the standard deviation $\sigma(r)$ are taken from a fixed environment of r. The membrane of a cell is characterised by a significant change of $\mu(r)$ and a raise of $\sigma(r)$. A third component $d(r)$ is constantly decreasing the bigger the distance between r and the origin gets. This component was introduced, because in the extracellular space may exist structures satisfying the two graylevel criteria even better than those pixels r close to the cell membrane. The linear factor $d(r)$ decreases the propability in radial direction supporting pixels with significant change in $\mu(r)$ and large $\sigma(r)$, the more they lie in the inner of the cell. The three components have to be weighted individually and can be adapted to the cytological images by the user, even if the microscopies are inhomogeniously illuminated.

Of course, this simple method is not capable to detect cell membranes with satifying quality, but if a sufficient number of profiles is generated, it yields approximations $m_\varphi \in r_\varphi$ that are suitable to obtain important image features. Now the mean graylevel μ_{in} and standard deviation σ_{in} of all pixels $\{b(r_\varphi)|r \leq m\}$ is calculated. These are used to construct the energy levels $l(g)$.

The inner of an object should not influence the expansion of the deformable membrane that is inflated by a constant pressure. The higher the energy level $l(g)$, the stronger is the counterpressure that graylevel g applies to the deformable membrane. Hence, for pixels inside the object the energy levels should equal 0. The range depends on σ_{in} and can be influenced by the user via a weighting factor w.

$$(\mu_{\text{in}} - w\sigma_{\text{in}}) \leq g \leq (\mu_{\text{in}} - w\sigma_{\text{in}}) \;\Rightarrow\; l(g) = 0 \tag{1}$$

The graylevels below and above the inner ones should act as barrieres, because they might occur at the border of the object. The slope of the energy levels to both sides of the plateau depends again on the standard deviation. The bigger σ_{in}, the lower is the slope and the higher is the tolerance for noisy graylevels. Fig. 2 shows a cytological sample and the according energy levels $g(l)$.

Applying a constant inner pressure to the deformable membrane, an initial determination of individual external forces F_g for different image material is required. The advantages of this dynamic approach, compared to common active contours, with external forces being determined solely by the image's gradients, are discussed in Sec. 5. The weights of such screening methods are subject to optimization by the user. In practice, only a feasable number of control parameters have to be adapted, because most of them reveal to be of minor importance.[16]

2.3. The Deformable Membrane Model

The main module is the deformable membrane itself. For its algorithmic realization the data representation of the contour, the applied internal and external forces, the iterative movement, and a consistency check (Sec. 2.3.1) had to be developed. The active contour to be described in this section, simulates the behaviour of a biological membrane, that is adapted to an object's shape by the influence of a constant internal pressure. Generally, the model is capable

to find inner contours by expanding and outer contours by shrinking of the deformable membrane. In the following we will only describe the expanding case, because the mechanisms are more intuitive and the shrinking case can be derived from this.

A membrane consists of a set of vertices $V_1, V_2, \ldots, V_n$ and edges $\vec{d}_1, \vec{d}_2, \ldots, \vec{d}_n$. Their deterministically predefined behaviour corresponds to the dynamics of physiological membranes. The membrane is closed: $V_{n+1} = V_1$.

2.3.1. Consistency check of the membrane

The different forces applied to the vertices V_i may lead the membrane into inconsistent states. The following three situations are detected as inconsistencies:

- ▷ Edges $\vec{d}_i = \overrightarrow{V_i, V_{i+1}}$ that are longer than a predefined maximal length will be split and a new vertex $V_{i'}$ with a new edge $\vec{d}_{i'} = \overrightarrow{V_{i'}, V_{i+1}}$ is inserted. Then $\vec{d}_i$ is modified to $\overrightarrow{V_i, V_{i'}}$.
- ▷ A vertex V_i, whose adjacent edges $\vec{d}_{i-1}$ and $\vec{d}_i$ are both smaller than a predefined minimal length will be removed together with its edge $\vec{d}_i$. The remaining edge $\vec{d}_{i-1} = \overrightarrow{V_{i-1}, V_{i+1}}$ will fill the gap.
- ▷ Contour errors like loops resulting from distortions in the image background are dissolved by removing the looping segment.

These checks guarantee the physical consistency of the mathematical model. For each iteration a membrane with regularly distributed vertices is provided.

2.3.2. The driving forces

In order to simulate the behaviour of physiological membranes, their mechanical properties were incorporated.[17] Hence, only principles from mechanics and statics were used to make up the dynamics of the microscopic membrane model. The principle is that influences resulting from the image's graylevels are applied to the edges. The sum of all such influences on two edges $\vec{d}_{i-1}$ and $\vec{d}_i$ imposes a force to the vertex V_i. The vertex is moved as soon as all driving forces are known.

During the iterative process veritices can reach a stable state, where all forces are in balance. Such vertices are frozen and will remain at their current position. Of course, frozen vertices have a stabilizing effect on their neighbours. If all vertices have reached a stable state, the membrane model has converged. This corresponds to an implicit annealing process, with the temperature (imposing the contour's dynamics) being constantly decreased until the system converges into a stable state.[18]

The model is initialized by a start contour consisting of only a few vertices and edges. The initial contour $C(0)$ is centered around a given point within the object (e.g. the center of the image). At this point, the various forces begin to impose the membrane's dynamics:

- ▷ A constant *internal pressure* is applied to each edge during the complete process. This results in a force F_p^i that is the product of the internal pressure and the length of $\vec{d}_i$ (Fig. 3a).
- ▷ An edge $\vec{d}_i$ picks up *external influences* from the image. At each point of an edge, the weighted energy levels of the pixels lying perpendicular inwards and outwards are summed up. The graylevel have to be interpolated, because the pixels to be read might not correspond to the discrete image grid. The weighting is performed by a hyperbolic function, that weakens the energy levels for increasing distance to $\vec{d}_i$. The total difference between the energy levels of both sides of $\vec{d}_i$ is interpreted as a potential and applies an force F_g^i to each point of $\vec{d}_i$ in normal direction.
- ▷ The amount of *contour deformation* is modeled by an additional force F_d. The lipids of physiological cell membranes stick together by van–der–Waals bindings. They have no tension elasticity but resist deformations. This means, that for given surface and area of a cell, its membrane minimizes the second order derivative, which is the state of least deformation energy. For minimizing the second order derivative at a vertex V_i two situation have to be distinguished:

- The edges in the environment of V_i are still active: A deformating force F_d draws V_i towards the mean coordinate of the membrane section $V_{i-2}, V_{i-1}, V_i, V_{i+1}, V_{i+2}$. This simple method reduces the second order derivative of the contour (Fig. 3b).
- In the environment of V_i are stable edges: In this case, the shape given by the already frozen edges is completed by following their mean direction vector (Fig. 3c).

The minimzation of the membrane's second derivative leads to a smoothly interpolated shape. Even if the contour information in the digital image is incomplete, the natural behaviour of the menbrane determines contour information by propagating information from the ambiguous parts of the contour.

While F_d is applied to vertices, F_p and F_g are applied to edges. The latter ones are transformed into vertex forces, to obtain a resulting force for the vertex movement. Therefore, the constant internal pressure F_p and the normal force F_g^i contribute to a momentum that is applied to the adjacent vertices V_i and V_{i+1}. At each vertex V_i the momentum results in a *supporting force* F_s^i perpendicular to the corresponding edge (Fig. 3a). F_s is applied to the vertex V_i. A vertex V_i picks up the resulting force $F_{\text{res}} = F_s^{i-1} + F_s^i + F_d$ whose amount and direction detemines the movement of V_i (Fig. 3d). Hence, only the vertices are moved while the edges are given implicitly by their adjacent vertices. The vertices can be supposed to have no mass and no momentums of inertia.

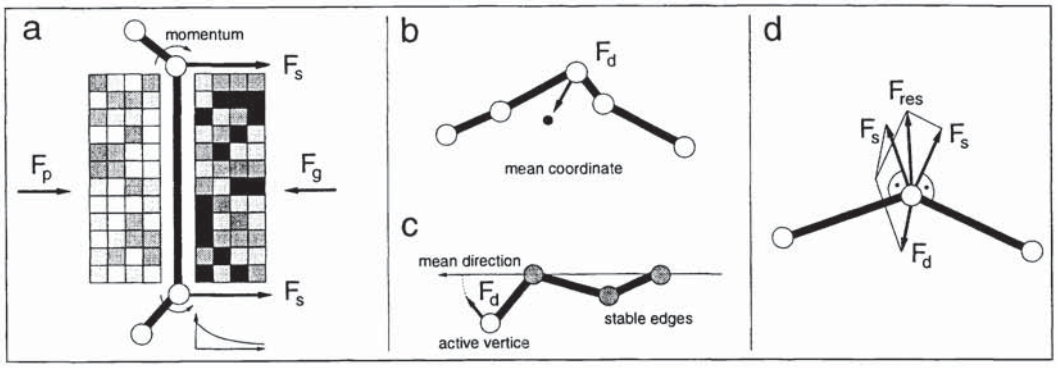

Figure 3. The forces F determine the membrane dynamics. (a) visualizes the contrary forces that are applied to edges: the internal pressure F_p and the image dependent external force F_g. The two cases to be distinguished for the application of the deformating force F_d, are shown in (b) and (c). The various forces applied to a vertex culminate in its movement determined by the vectorial sum F_{res} (d).

2.3.3. Termination of the contour detection

A vertex V_i reaches a stable state if it hasn't moved significantly during the last iterations. This means that the applied forces are more or less in balance. The position of solidity determines the cell boundary. A stable vertex has a stabilizing effect on neighbouring vertices by the deformation force F_d. Frozen vertices reduce the dynamical range of their neighbours. If all vertices have reached a stable state, the algorithm converges. This corresponds to an implicit annealing process if the vertex movements are interpreted as temperatures.

Nevertheless, constellations may occur where single vertices will never reach stability, even though all neighbours are already frozen. Such situations occur for oscillating instabilities or cytological structures that partly doesn't contain sufficient gradient information (e.g. neurons with dedrites running out of the image). Therefore, the maximal number of iterations can be restricted by the user.

2.4. Stochastic enhancement of the contour

The deformable membrane algorithm might not detect the shape of cytological material precise enough for subsequent quantifications. A contour that was found by the membrane model is based on a balance of internal and external forces. Usually, there is a non–constant gap between the converged contour and the actual contour of the cell as a human observer would have determined it. Therefore a further enhancement of the contour is required. The contour

is adapted to local graylevels by a stochastic approximation, which determines the position of vertices by a maximum norm.

In terms of optimization theory, the deformable model has converged into a local optimum by analytical principles, and yields an approximation of the actual cell contour. The subsequent undirected stochastic enhancement is capable to escape from local optima and find even better optima with respect to the same conditions and forces the deterministic deformable model uses. This is achieved by small randomly selected translations of single vertices. If a translation leads to an increase of the given quality criterion, the vertex is moved, otherwise it will remain at its current position. The quality of a vertex V_i consists of the following components:

- ▷ To incorporate the influences of the adjacent edges $\vec{d}_{i-1}$ and $\vec{d}_i$, the external force F_g^i contributes positively to the detection quality. A large external force corresponds to high propability of being not in the intracellular space anymore.
- ▷ High deformation forces F_d^i that signal the existence of tensions in the contour, contribute negatively to the detection quality. Strong contour deformations are unwanted because physiological membranes have small second order derivatives.
- ▷ Additionally, the deformation forces of the neighbouring vertices F_d^{i-1} and F_d^{i+1} contribute negatively to the detection quality of the vertex V_i.

The three components have to be weighted by the user in advance. This guarantees an optimal detection quality for screening experiments. The effect of the stochastic post–processing of the membrane is shown in Fig. 4. For all images the number of iterations of the stochastic adapation is set to 3000. A more intelligent termination criterion has not been implemented yet. In average, every sixth alternation of a vertex increases its local detection quality and is therefore performed. This number might give an idea of the usefullness and positive effects of the stochastic contour enhancement.

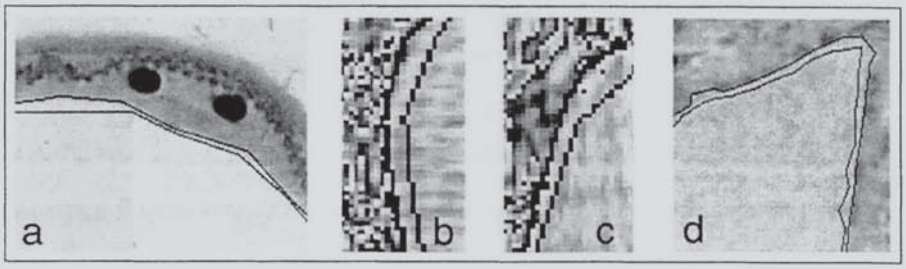

Figure 4. The effect of the stochastic enhancement is shown by four examples. The inner contours towards the homogeneous graylevels (intracellular space) is obtained by the deformable membrane. The outer contours, that are far better adapted to local graylevels, result from the subsequent stochastic enhancement.

3. LOCAL CONFIDENCE OF A CONTOUR

However, automatic algorithms cannot detect biological material with the same exactness than experts can. Especially inhomogeneous illumination (for light microscopes) and varying staining concentration due to chemical tissue properties lead to inexact detection results. To meet the requirements of quantitative cytology, a measure of confidence is provided by the algorithm that gives the local detection quality of the enhanced contour at each edge $\vec{d}_i$. The local confidence can be regarded as propability of detecting the correct parts of the image as separation between different tissue types. The providence of such a local detection quality enables the extraction of robust quantitative results from contours containing minor errors and irregularities.

To determine the local confidence, an initial value of $c_i = 1$ is assumed for an edge $\vec{d}_i$. Certain criteria are defined, each of which reducing c_i if it is not fullfilled. This equals fuzzy logic techniques, because each edge is provided with

the propability of being in the state of perfect detection.[19] In contrast to the usual arithmetic rules of fuzzy logic, we use the product of two values and not their minimum as AND operator. To obtaint c_i, several multiplications by factors ≤ 1 are calculated:

- In a certain range of $90 \pm \beta_1$, where is hardly any curvature, thus a small second order derivative, the local shape is most likely correct. But if an angle exceeds $90 \pm \beta_2$ the curvature is so large, that an unphysiological bend occurs, which is most likely a detection error. The factor f_a^i uses the two angles at the vertices V_i (angle with predecessing edge) and V_{i+1} (angle with successing edge). The two external parameters $\beta_1 < \beta_2$ direct the decay of f_a^i. For all angles $90 - \beta_1 \leq \alpha \leq 90 + \beta_1$ the factor f_a^i will not be reduced. If the angle $\alpha < 90 - \beta_2$ or $\alpha > 90 + \beta_2$ the edge $\vec{d_i}$ is evaluated as being wrong, by setting $f_a^i = 0$. The range between these two thresholds is linearly interpolated on either side.

- The factor f_g^i evaluates the graylevel gradient Δ along the edge $\vec{d_i}$ in perpendicular direction. In most cases, the cell membranes are determined by stained tissue. This information might be incomplete due to staining irregularities. The stronger the gradients are, the more likely is the edge $\vec{d_i}$ a correctly detected section of the natural cell membrane. Again, in between an externally controlled range $\Delta_{\text{lo}} \leq \Delta \leq \Delta_{\text{hi}}$, the gradient leads to a linearly decreasing factor f_g. Gradients $\Delta > \Delta_{\text{hi}}$ lead to $f_g = 1$, while $\Delta < \Delta_{\text{lo}}$ leads accordingly to $f_g = 0$.

- The third factor f_s^i is given by

$$f_s^i = \frac{2 \cdot f_a^i f_g^i + f_a^{i-1} f_g^{i-1} + f_a^{i+1} f_g^{i+1}}{4} \tag{2}$$

  to smooth the local confidence c_i by incorporating the neighbour confidences. This is useful since the detection quality will not change rapidly from one edge to its neighbour, thus f_s^i aims to reduce errors in the confidences c_i.

Hence, the total confidence c_i for edge $\vec{d_i}$ is given by $c_i = f_a^i \cdot f_g^i \cdot f_s^i$.

Figure 5 shows two detection results and their local confidences. The local confidence can be used profitably if features concerning the membrane of biological objects are to be quantified. For example, if the mean curvature of a cell determines its deformation, or the total staining of the membrane is proportional to the occurance of special structures like synapses of receptors.

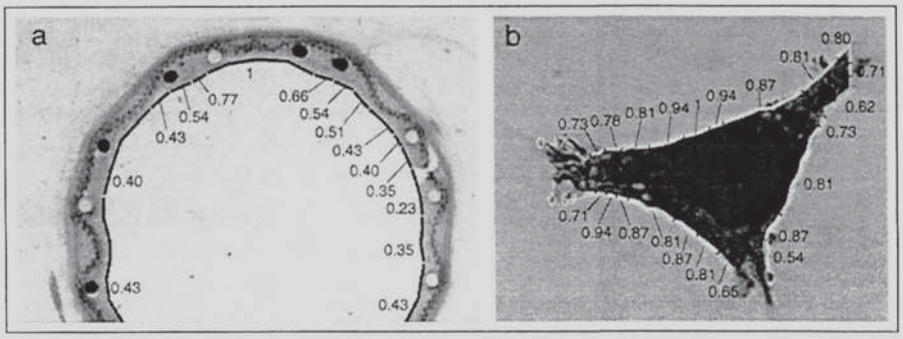

Figure 5. The evaluation of the detection quality is exemplified in this figure. In (b) the local confidences c_i are graylevel coded. h The higher c_i, the lighter is the according edge $\vec{d_i}$. One can see, that the attached local confidences correspond to the detection quality, because clear edges are rated high, while ambiguous edges are rated rather low.

4. APPLICATIONS OF THE METHOD

The deformable membrane model was successively adapted to different applications. They prove the suitability of the method for different microscopic problems. All adapations can be made quickly by an experianced user. The configurations are stored in a database and can be recovered and used as a basis for the adaptation of the algorithm to similar problems.

4.1. Resorbable nets made of a biomaterial

For the assessment of biomaterials that can be used to cover wounds in operations, the decrease of the covered area of resorbable nets has to be quantified. The detection of the material section in the microscopic samples is shown in Fig. 6.

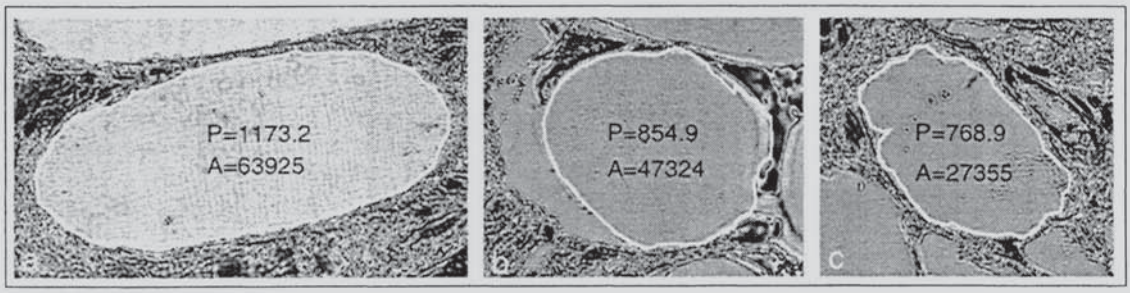

Figure 6. Three sections of a resorbale net are detected by the deformable membrane. The subsequent quantification module determines area A and perimeter P of the detected regions.

4.2. Metal stents in blood vessels

Fig. 7a shows an intersection of a blood vessel with implanted metal stents (dark structures), preventing the closing of the vessel. The assessment of the biocompatibility of the used stent material can be done via the thickness of the neointima, that is the innermost tissue section of the vessel. The thickening of the neointima is a direct pathological aberation caused by the used material and has to be quantified.

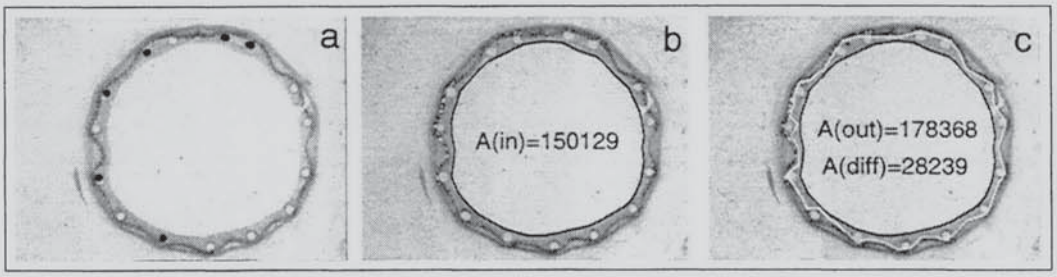

Figure 7. The blood vessel with implanted stents is shown in (a). The inner contour of the neointima is shown in (b), while in (c) both contours are given. the difference $A(\text{diff}) = A(\text{out}) - A(\text{in})$ determines the area covered by the neointima.

This is an example for the flexible use of the deformable membrane, because different configurations have to be used to detect the two borderlines of the neointima. The dark spots in the vessel tissue have to be removed first, for they represent high barriers for the membrane model. They are detected by means of morphological filters and replaced by the mean inner graylevel. In a two stage detection, the inner edge of the intima is detected first. The detected inner border is used as a start contour for a second run with a specially adapted configuration. The difference of both areas is the covered area of the intima. Using the known radius, the mean thickness of the intima is obtained, which is proportional to the biocompatibility of the stent material.

4.3. Rat motoneurons after lesion

The detection of motoneurons of rats by means of the deformable membrane model is shown in Fig. 8. The pathologic aberations caused by a lesion of the spinal cord can be evaluated by the occurance of synaptic boutons on the membrane of a neuron. The stained boutons can be seen as little dark spots in the membrane (Fig. 8a). After the detection of the neuron's membrane (Fig. 8b) it is extracted as region–of–interest (Fig. 8c) and the synaptic boutons are segmented by a local thresholding technique. The morphological analysis yields boutons of decreasing sizes by differently sized morphological openings.[20] This gives valuable information on the occurance and density of the boutons in the cell membrane. Other quantitative parameters like mean coverage and entropy of the boutons are weighted by the corresponding confidence factors.

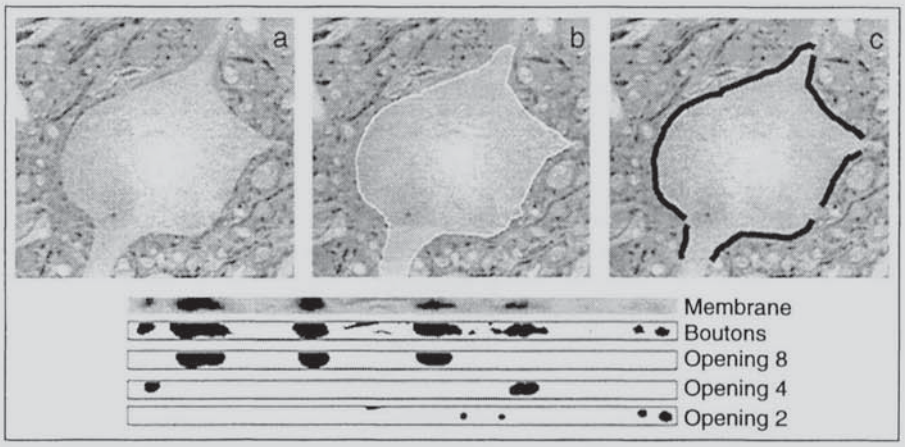

Figure 8. The application of the deformable membrane on rat neurons (a) yields its contour (b). The parts of the membrane with sufficient confidence are supposed to contain verified information and are extracted (c). The analysis of attached synaptic boutons is performed by means of morphological filters, and yields quantitative parameters for the assessment of pathological aberations.

4.4. Toxic reaction of L–929 mouse fibroblasts

For the evaluation of cytotoxicity of biomaterials, the morphology of fibroblasts, that were in defined contact with the material, has to be quantified. If a biomaterial extract has toxic effects, the fibroblasts show pathological aberations of their shape. Therefore, parameters like compactness and mean local curvature have to be extracted to describe the shape of an object quantitatively. Fig. 9 show those edges of the detected contours of three fibroblasts, with a local confidence $c_i > 0$. The mean local curvatures α_C is the normalized confidence–weighted sum of all local curvatures, given by the angles between two edges. Additionally, the mean confidence $\overline{C}$ of the contour yields a measure for the detection quality of the cell.

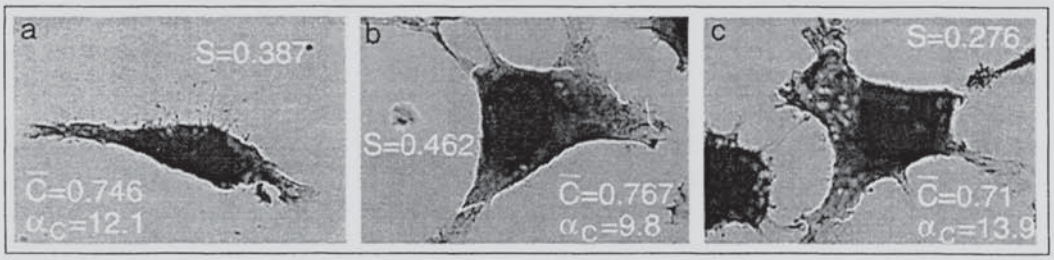

Figure 9. The contours of three fibroblasts are shown. Edges with $c_i = 0$ are not displayed, for they do not contribute to the confidence–weighted mean local curvature α_C of a cell. α_C is normalized by the mean confidence $\overline{C}$ of the contour. The formfactor S quantifies the compactness.

The formfactor[3] $S = 4\pi A/P^2$ is a measure of compactness and is also a means to quantify the morphological aberations of a cell caused by the biomaterial. The circle as ideal object has the formfactor $S = 1$, other geometric shapes have formfactors $S < 1$ depending on the irregularity of their shape. The inverse proportional relation between S and α_C is obvious, because less compact objects have more curved borders.

5. CONCLUSIONS

The deformable membrane model was specially developed for the segmentation of biological objects, that were aquired on microscopical scale.

Its characteristic design was given by the mechanisms responsible for the dynamics of physiological membranes. This implies that features like elasticity are not needed. Often, spline techniques are used to interpolate between vertices.[21] This approach was not realized either, because the computational costs were not appropriate in our eyes. Additionally, there is no corresponding mechanism for splines in membrane mechanics. Since density of vertices can be adpted, satisfying results can be achieved for a large field of applications.

In contrast to common active contour approaches a constant internal pressure is applied to model the self–dynamics of the membrane resulting in a preferred search direction. The algorithm can easily be modified to a shrinking membrane, driven by an external pressure. This is enabled by energy levels, providing the necessary information to prevent the convergence of the self–driven contour within the object. In comparison to methods with an external force given solely by local gradients,[22] our approach has the advantage that a fairly good approximation is not needed as starting contour $C(0)$. Such a–priori requirements are reduced to a single point lying within the object of suspicion. The deformable membrane is converging to a stable state, where the dynamics stops due to the balance of the applied forces. The use of a self–driven membrane corresponds to a deterministic annealing process. However, the extension to stochastic annealing improves the results (Sec. 2.4).

The method is especially suitable for screening of large cell populations because it is fully automated, but a supervisor can control the quality of the results via specially generated session protocols. The dynamics of the membrane and the various pre– and post–processing steps is controlled by about 40 parameters. For the adaptation of an existing configuration onto a special problem, in the majority of cases only five of them need to be newly determined. These are the slope of the energylevel fuction $l(g)$, the constant internal pressure, the hyperbolic function weighting the graylevel range of an edge for the determination of F_g, and the maximal and minimal length of the edges.

ACKNOWLEDGMENTS

This work was done within the framework of the *Interdisciplinary Center of Research on Biomaterials* (IZKF "Biomat"), Aachen University of Technology (RWTH), Aachen, Germany. The funding of the Federal Ministry of Education, Science, Reseach, and Technology (BMBF Grant No. 01ks9503/9) is gratefully acknowledged.

The authors would like to thank Dr. B. Klosterhalfen, Dr. W. Nacimiento, and Dr. K. Schürmann (all with the Faculty of Medicine, RWTH Aachen) for their contributions.

REFERENCES

1. I. Young, "Quantitative microscopy," *IEEE Engineering in Medicine and Biology* **15**(1), pp. 59–66, 1996.
2. S. Ong, X. Jin, Jayasooriah, and R. Sinniah, "Image analysis of tissue sections," *Computers in Biology and Medicine* **26**(3), pp. 269–279, 1996.
3. J. Russ, *Computer–Assisted Microscopy*, Plenum Press, New York, 1990.
4. C. Glasbery and G. Horgan, *Image Analysis for the Biological Sciences*, Wiley & Sons, Chichester, 1995.
5. C. Garbay, "Image structure representation and processing: A discussion of some segmentation methods in cytology," *IEEE Trans. Pattern Analysis and Machine Intelligence* **8**(2), pp. 140–146, 1986.
6. C. Liedke, T. Gahm, F. Kappei, and B. Aeikens, "Segmentation of microscopic cell scenes," *Analitical and Quantitative Cytology and Histology* **9**(3), pp. 197–211, 1987.
7. C. Murray and M. O'Malley, "Segmetation of plant cell pictures," *Image and Vision Computing* **11**(3), pp. 155–162, 1993.

8. K. Wu, D. Gaultier, and M. Levine, "Live cell image segmentation," *IEEE Biomedical Engineering* **42**(1), pp. 1–12, 1995.
9. P. Belhomme, A. Elmoataz, P. Herlin, and D. Bloyet, "Generalized region growing operator with optimal scanning: Application to segmentation of breast cancer images," *Journal of Microscopy* **186**(1), pp. 41–55, 1997.
10. C. MacAulay and B. Palcic, "A comparison of some quick and simple threshold selection methods for stained cells," *Analytical and Quantitative Cytology and Histology* **10**(2), pp. 134–138, 1988.
11. E. Breen, "Regression methods for automated colour image classification and thresholding," *Journal of Microscopy* **174**(1), pp. 23–30, 1994.
12. S. Lobregt and A. Viergever, "A discrete dynamic contour model," *IEEE Trans. Medical Imaging* **14**(1), pp. 12–24, 1995.
13. A. Chakraborty, L. Staib, and A. Duncan, "Deformable boundary finding in medical images by integrating gradient and region information," *IEEE Trans. Medical Imaging* **15**(3), pp. 859–870, 1996.
14. A. Yezzi Jr., S. Kichenassamy, A. Kumar, P. Olver, and A. Tannenbaum, "A geometric snake model for the segmentation of of medical imaginery," *IEEE Trans. Medical Imaging* **16**(2), pp. 199–209, 1997.
15. N. Otsu, "A threshold selection method from grey level histograms," *IEEE Trans. Systems, Man, and Cybernetics* **9**, pp. 62–66, 1979.
16. W. Mesker, J. v.d.Burg, P. Oud, C. Knepfle, M. Ouwerkerk-v.Velzen, N. Schipper, and H. Tanke, "Detection of immunocytochemically stained rare events using image analysis," *Cytometry* **17**(3), pp. 209–215, 1994.
17. U. Seifert, K. Berndl, and R. Lipowski, "Membrane bending energy and determination of phosphorlipid shape, vesicles, and red blood cells," *Physical Review A* **44**, p. 1182 ff, 1991.
18. D. Rückert, P. Burger, S. Forbat, R. Mohiaddin, and G. Yang, "Automatic tracking of the aorta in cardiovascular MR images using deformable models," *IEEE Trans. Medical Imaging* **16**(5), pp. 581–590, 1997.
19. D. Dubois and M. Jaulent, "A general approach to parameter evaluation in fuzzy digital pictures," *Pattern Recognition Letters* **6**, pp. 251–259, 1987.
20. R. Haralick, S. Sternberg, and X. Zhuang, "Image analysis using mathematical morphology," *IEEE Trans. Pattern Analysis and Machine Intelligence* **9**(4), pp. 532–550, 1987.
21. D. Rückert and P. Burger, "A multiscale approach to contour fitting for MR images," in *Procs. SPIE*, No. 2710, pp. 289–300, 1996.
22. M. Kass, A. Witkin, and D. Terzopoulos, "Snakes: Active contour models," in *First Intern. Conf. on Computer Vision*, pp. 259–269, 1987.